08

SQIF magnetometer for navigation systems: experimental and theoretical study of base cells

© *G.S. Khismatullin,*[1,2] *N.V. Kolotinskiy,*[3] *M.M. Khrenov,*[1,2,4] *A.S. Ionin,*[2] *M.Yu. Fominsky,*[4] *L.V. Filippenko,*[4] *I.I. Soloviev,*[1,4] *N.V. Klenov*[3]

[1] Skobeltsyn Institute of Nuclear Physics, Moscow State University,
119991 Moscow, Russia
[2] Russian Quantum Center,
143025 Moscow, Russia
[3] Moscow State University,
119991 Moscow, Russia
[4] Kotelnikov Institute of Radio Engineering and Electronics, Russian Academy of Sciences,
125009 Moscow, Russia
e-mail: nvklenov@mail.ru

Received May 5, 2025
Revised May 5, 2025
Accepted May 5, 2025

The article is devoted to the development of a magnetometer to improve the accuracy of inertial navigation systems with superconducting gyroscopes. To minimize signal reading errors, a magnetometer design based on a chain of sequentially connected two-junction variable area interferometers (SQIF) is proposed, which solves the problem of dynamic range and „zero“ determination by magnetic field. The experimental part of the work includes the design and fabrication of test samples of interferometers, measurement of their static and dynamic characteristics, including voltage-flux dependencies. Numerical and analytical approaches have been developed to analyze the characteristics of the manufactured structures in order to adequately interpret the data obtained and improve the technology. The obtained results confirm the promising nature of the selected approaches and the high potential of the proposed theoretical methods for the analysis of the peculiarities of macroscopic quantum interference.

Keywords: Josephson effect, two-contact interferometer, SQIF, gyroscope.

DOI: 10.61011/TP.2025.09.61930.99-25

Introduction

Recently, superconducting quantum interference device (SQUIDs), usually consisting of a superconducting circuit with a pair of weak connections called Josephson junctions, have been actively used in various navigation systems. Their exceptional sensitivity to weak magnetic fields makes them particularly in demand when developing new types of autonomous and combined inertial systems, as well as for high-precision geolocation of mobile objects.

A superconducting navigation system necessarily includes a gyroscopic part, which makes it possible to calculate coordinates (an inertial system), i.e. it allows you to determine the angular velocities of the object on which it is located, and therefore the change in its position over time relative to a known initial position.

Gyroscopes using SQUID magnetometry can be divided into two subclasses, depending on the presence or absence of moving parts. Superconducting navigation systems without moving parts, in particular, SARDIN [1] and the interferometric accelerometer [2] demonstrate high sensitivity (for example, see [2], the predicted acceleration sensitivity is $\sim 10^{-10}\ \frac{\mathrm{m}}{\mathrm{s}^2\sqrt{\mathrm{Hz}}}$. Nevertheless, even such characteristics turn out to be worse than those of superconducting gyroscopes with moving parts.

Superconducting gyroscopes with moving parts represent a development of the ideas underlying electrostatically suspended gyroscopes [3]. Initially, such a gyroscope was proposed in Ref. [4] to test the general theory of relativity in the Gravity Probe experiment [5].

The principle of operation of this system is based on the features of the superconducting state, when Cooper pairs of electrons act as the main charge carriers. The condensate from these pairs is able to shift relative to the ions of the crystal lattice without loss of energy (without „friction“), which means the formation of a dissipative supercurrent. When the suspended superconducting sphere (gyroscope) begins to rotate, the Cooper pair condensate remains stationary. At the same time, the uncompensated rotation of the charged ions of the crystal lattice creates a magnetic moment, which turns out to be directed along the axis of rotation of the gyroscope and retains its orientation in space. This magnetic moment can be measured with high accuracy using a magnetometer, which also makes sense to use a superconducting and sensitive SQUID [6].

The obtained characteristics of such gyroscopes exceed the capabilities of most competitors. In particular, the bias

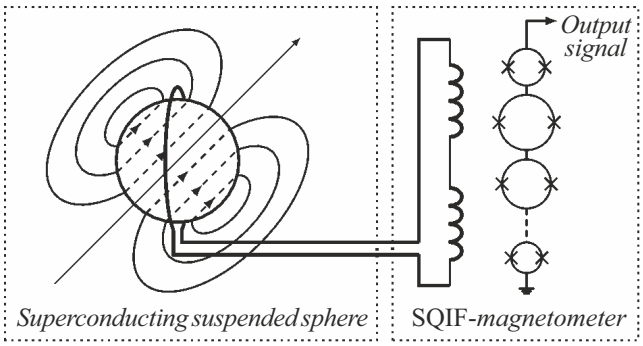

Figure 1. Diagram of a superconducting gyroscope with a movable part consisting of a suspended superconducting sphere (left) and a SQIF magnetometer based on series-connected two-contact SQUIDs (right).

stability can be theoretically increased to $10^{-11}\ ^{\circ}/\mathrm{h}$, and the experimentally confirmed value is $10^{-4}\ ^{\circ}/\mathrm{h}$ [3,6].

We propose in this paper an approach to modifying a SQUID magnetometer, which is a key element of a gyroscope along with a superconducting sphere. The magnetometers we are interested in can be implemented not only on the basis of single SQUIDs, but also on the basis of parallel or serial arrays of SQUIDs providing a significantly larger dynamic range (see, for example, the review in Ref. [7]). However, despite the obvious advantages, SQUID magnetometers face a number of technical limitations, the main of which is the problem of returning the operating point (de-jumping) [7].

Indeed, due to the frequency of the SQUID magnetometer voltage response function, any strong or rapid effect on it can cause parasitic output voltage surges. Such parasitic jumps increase the magnitude of the angular random walk (AWR), which, in turn, leads to an increase in positioning errors over time t as $t^{5/2}$ [8]. Various solutions have been proposed to overcome this problem, for example, using SQUID cascades [9].

Nevertheless, we believe that the abandonment of the periodicity of the voltage response function to the magnetic flux is the most promising solution to overcome this flaw. This feature can be obtained by using an array of series-connected two-contact interferometers with effective areas varying within specified limits — serial SQIF structures (superconducting quantum interference filters) (Fig. 1) [10]. Their use as part of navigation systems will improve the accuracy of measurements during long-term operation in various external conditions.

The structure of the article is as follows: first, we consider the process of designing cells of serial SQIF structures, then we describe a procedure in which important, but not directly measurable characteristics (the spread of critical currents of the resulting Josephson junctions, real inductance of circuits) can be obtained based on the results of experimental research using numerical simulation. Finally, we present an analytical theory for quickly calculating the voltage-flux characteristics of large SQIF structures and verify its adequacy when compared with measurement data.

1. Design and manufacture of magnetometer base cells with different effective areas

The key scientific and technical problem to be solved in this work is the problem of reproducible technology for creating SQIF magnetometer cells, and not all important cell characteristics are easy to measure directly. One of the main characteristics of a two-contact DC SQUID, which is closely related to its effective area and determines, among other things, its sensitivity to changes in the external magnetic field, is the inductance of the interferometer circuit. Therefore, the most important step in the research was the development of a methodology for the experimental evaluation of this value on real test samples.

The basis for determining the inductance of DC SQUIDs (as well as the inductance per square of the thin superconducting films used, which is one of the main parameters of the technology used), we propose to use the measurement of the modulation period of the voltage-flux characteristic of the SQUID. Test two-contact SQUIDs with different areas were designed and manufactured to test the approach. Fig. 2 shows the topology of a DC SQUID based on the niobium technology of the Kotelnikov Institute of Radioengineering and Electronics of RAS [11]. The thicknesses and materials of the layers from which the integrated circuits are made are also shown in the figure. The device is located above a superconducting screen made of niobium, and the effective external magnetic flux in this case is set using a control line lying in the SQUID plane. A section of the niobium film in the M2 layer, the inductance of which can be determined experimentally, is outlined with a red dashed line. This area has a size of 1 square in this example. SQUIDs in which the area of the studied area is 2, 3, 4 and 5 squares will be also considered in this paper.

It is well known [12] that the value of the maximum supercurrent flowing through the SQUID periodically depends on the applied external magnetic flux, and the modulation period is Φ_0 (quantum of magnetic flux). Using this property of interferometers, it is possible to measure the values of unknown inductors by embedding these sections in the inductive loop of the interferometer, and measuring the modulation period of the total supercurrent or voltage. The disadvantage of this method is that the inductance measured in this way will be mutual, not its own, since the control line is not connected to the SQUID loop.

In order to measure the own inductance of the area of interest, an approach was proposed in Ref. [12], which consists in the fact that the control line for setting the magnetic flux through the SQUID should be directly

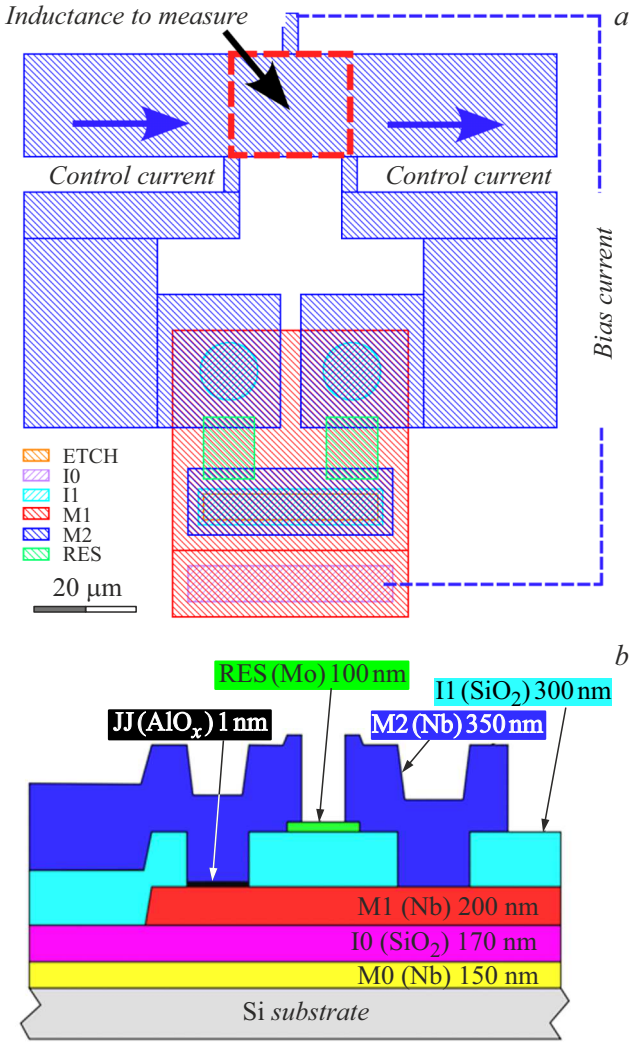

Figure 2. *a* — topology of a DC SQUID consisting of two identical shunted Josephson junctions superconductor/insulator/superconductor (SIS) based on a three-layer Nb/AlOx/Nb structure with a critical current density of 0.1 kA/cm^2. The critical junction currents in the project are the same and should be 100 μA. The resistances of the resistive shunts are also the same and should be 0.3 Ω; *b* — schematic representation of the structure of the shunted Josephson junction above the screen. The diagram shows the names, materials of the layers and their thicknesses used in the Kotelnikov Institute of Radioengineering and Electronics of RAS.

connected to the loop of the interferometer. In this case, the section whose inductance needs to be measured is, in fact, itself a section of the control line. The value measured in this way will be the own inductance of this section.

The experimentally determined values of the inductance per square were compared with the values obtained when modeling the studied topologies in the 3D-MLSI program [13]. The inductance of one square of the superconducting film located above the superconducting screen obtained in this calculation was 0.72 pH.

2. Numerical simulation for extrapolation of cell parameters based on experimental results

SQUIDs with five different effective areas were selected for analysis. A photo of one of the produced cells and its equivalent circuit are shown in Fig. 3.

For such SQUIDs, the following values of the critical currents of the Josephson junctions were used in the design (J_1, J_2 in Fig. 3, *b*): Ic_1, $Ic_2 = 100\,\mu$A; the inductors ($L = L_1 + L_2$ in Fig. 3, *b*) were laid so as to obtain a value of 0.72 pH per square, and the values of the total inductances $L = L_1 + L_2$ were 0.72, 1.44, 2.16, 2.88, and 3.6 pH values for regions with areas of 1, 2, 3, 4, and 5 squares, respectively.

Fig. 4 shows an example of the developed design for the entire chip with the studied elements. Let's take a closer look at a single cell using the example of SQUID SQ1. The SQUID has two lines for setting the current (SQ1_+I and –I), two lines for voltage relief (SQ1_+V and –V), as well as two lines for setting the magnetic field by means of an external current through the inductors of the SQUID L_1, L_2. Thus, it is possible to measure the I-V curve $I(V)$, voltage-flux characteristics $V(\Phi)$, as well as the dependence of the critical current for the entire interferometer (i.e.

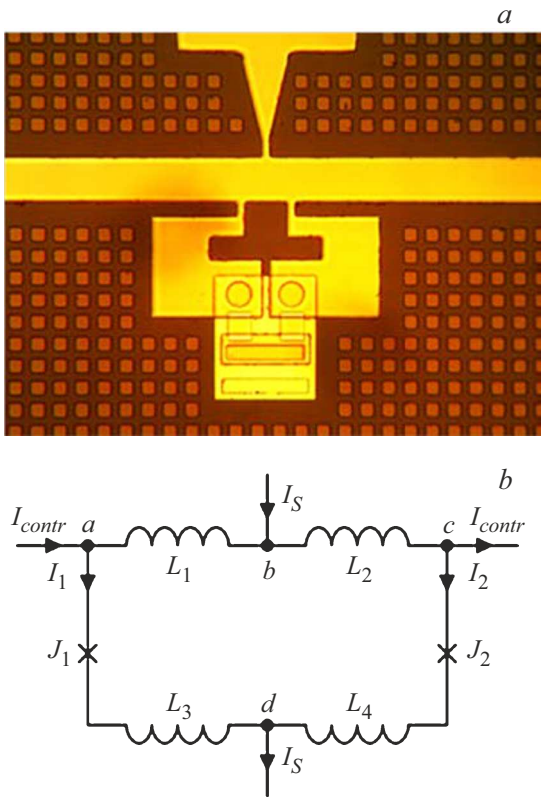

Figure 3. *a* — photo of the produced SQUID; *b* — equivalent circuit of the SQUID. The Josephson junctions *J*1 and *J*2 are marked by crosses. The total critical current of the SQUID is equal to the sum of the critical currents of the Josephson junctions: $I_{c1} + I_{c2}$; inductance of the SQUID circuit $L = L_1 + L_2 + L_3 + L_4$.

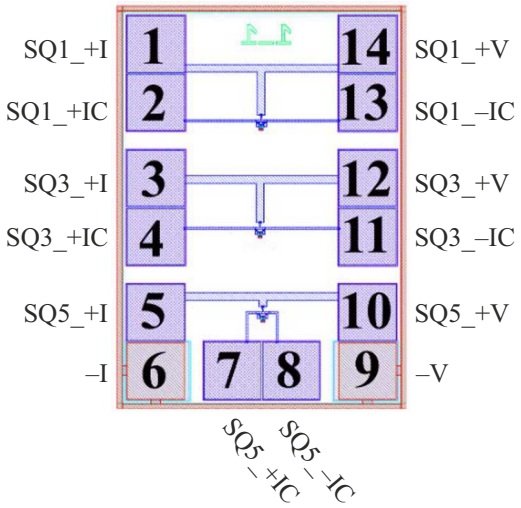

Figure 4. An example of a chip with three SQUIDs (SQ1, SQ3, SQ5).

the maximum dissipative current through the structure) from the magnetic field. Let's consider a methodology for determining the real characteristics of structures based on the analysis of such dependencies.

The following model was chosen for numerical analysis and extrapolation of important cell characteristics with equations based on Kirchhoff's rules and the balance of superconducting phases in the circuits:

$$\varphi_2 - \varphi_1 = 2\pi\varphi_a + \pi\beta_L\left(j - \frac{\alpha_L}{2}i\right), \qquad (1)$$

$$i = (1-\alpha_I)\sin(\varphi_1) + (1+\alpha_I)\sin(\varphi_2), \qquad (2)$$

$$2j = (1-\alpha_I)\sin(\varphi_1) - (1+\alpha_I)\sin(\varphi_2), \qquad (3)$$

where φ_1, φ_2 are phases at the Josephson junctions J_1, J_2; $I_{C0} = \frac{I_{c1}+I_{c2}}{2}$; $\varphi_a = \frac{\phi_a}{\phi_0}$ — normalized to the magnetic flux quantum ϕ_0 — flux through the SQUID circuit; $\beta_L = \frac{2LI_{c0}}{\phi_0}$; $j = \frac{J}{I_{c0}}$ — normalized circulating current in the SQUID; $\alpha_L = \frac{(L_1+L_3)-(L_2+L_4)}{(L_1+L_3)+(L_2+L_4)}$; $i = \frac{I}{I_{c0}}$; $\alpha_I = \frac{I_{c1}-I_{c2}}{I_{c1}+I_{c2}}$.

The experimentally obtained dependences of the maximum dissipative SQUID current on the applied magnetic field created by the flow of current I_{contr} through inductors L_1 and L_2 were approximated based on numerical modeling (Fig. 5). It can be seen that the quality of approximation of experimental data using simulation modeling is quite satisfactory. The proposed set of parameters in numerical modeling allowed us to obtain estimates for the following important characteristics, but not always amenable to simple direct measurement: the average critical current of the SQUID (I_{C0}), the inductive parameter β_L, as well as the asymmetry in critical currents $\alpha_I = \frac{I_{c1}-I_{c2}}{I_{c1}+I_{c2}}$, which is the essence of our methodology for the experimental evaluation of the production technology of superconducting structures. We obtained estimates for the key parameters from the analysis of experimental data and their comparison with

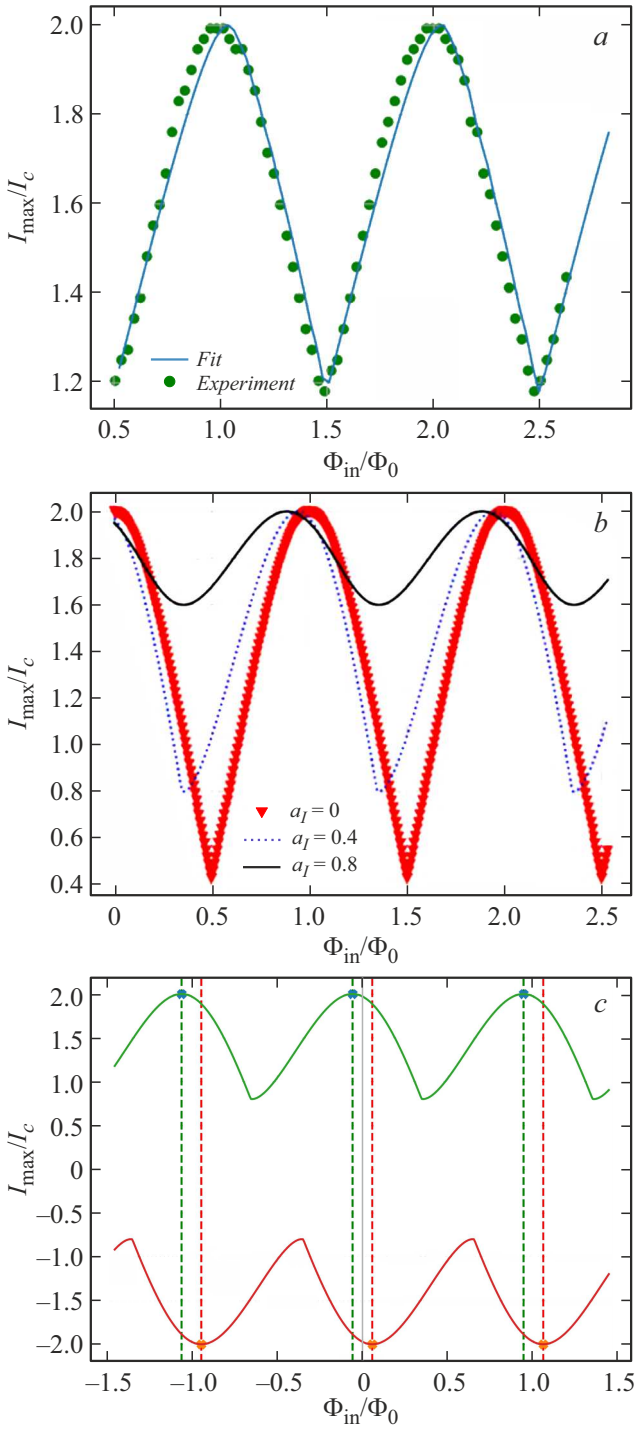

Figure 5. *a* — approximation (curve) of experimentally obtained data (points) on the dependences of the maximum dissipative current for a SQUID with an estimated inductance of 1.44 pH; *b* — calculated dependences of the maximum dissipative current on the magnetic flux applied to the circuit at different parameter values $\alpha_I = 0$; 0.4; 0.8 (triangles, dots, and a solid curve, respectively); *c* — the asymmetry of the dependence of the maximum dissipative current on the magnetic flux applied to the circuit at $\alpha_I = 0.4$.

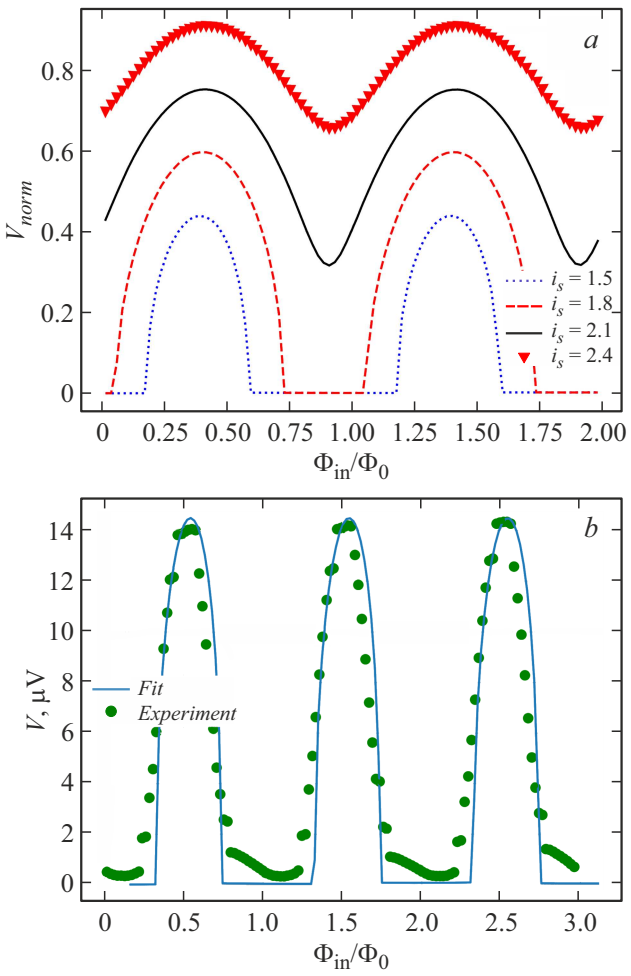

Figure 6. *a* — results of numerical calculation of the voltage-flux dependence at different normalized values of the displacement current i_s; *b* — experimentally measured voltage-flux dependence for a SQUID (point) and its numerical approximation (curve) with parameters $L_1 + L_2 = 3.08$ pH, $I_c = 86\,\mu$A, $\alpha_I = 0.25$.

modeling (see the example in Fig. 5, *a*): $L_1 + L_2 = 3.08$ pH, $I_{c0} = 86\,\mu$A, $\alpha_I = 0.25$ for the selected case. It can be seen that the most pronounced technological variation in the values of critical contact currents manifests itself in the asymmetry of current-flux dependencies, illustrated in Fig. 5, *c*.

For these parameters, we also present calculated voltage-flux dependences at different bias currents (Fig. 6, *a*), which shift the entire curve along the ordinate axis. Typical approximations of voltage-flux dependencies are also shown here, i.e., the dependence of voltage on the applied magnetic flux at a fixed value of the current setting the operating point (Fig. 6, *b*). When analyzing experimental data, it is impossible not to take into account the parasitic magnetic flux, which will lead to a shift in dependence along the abscissa axis.

As a result of applying the described technique, it turned out that the average value of the relative deviation of the measured critical current I_{C0} from the set value was -12% on 8 samples; the average value of the asymmetry α_I was approximately 0.13. The measured values of the inductance per square ranged from 0.74 to 0.8 pH, so that the relative deviation from the design value ranged from $\sim 3\%$ to 10%.

3. Analytical expressions for the interferometer response

Let us now consider an analytical approach to describing the measured transport characteristics of the SQUID [14], as well as comparing the analytical solution with the specified parameters with the final experimental result. In this case, the dimensionless current through the Josephson junction is represented as: $i_{1,2} = \sin(\varphi_{1,2}) + \dot{\varphi}_{1,2}$. The normalized inductance is $l = \frac{2\pi L I_{C0}}{\Phi_0}$. The normalized value of the SQUID voltage without taking into account the finite inductance will then be expressed as

$$v_{l=0}(i, \varphi_a) = \sqrt{\frac{i^2}{4} - (\cos(\varphi_a))^2}. \tag{4}$$

For the normalized voltage on the SQUID, taking into account the finite inductance, the following expressions should be used:

$$v_{l\neq 0}(i, \varphi_a) = v_{l=0}(i, \varphi_a) - A(i, l) L_s(i, l)^2 \times \frac{v_{l=0}(i, \varphi_a)^2}{L_s(i, l)^2 v_{l=0}(i, \varphi_a)^2 + 4} \left(\frac{i_b}{2} - v_{l=0}(i, \varphi_a) \right) \tan^2(\varphi_a). \tag{5}$$

The values $A(i, l)$, $L_s(i, l)$ can be expressed as follows:

$$A(i, l) = p(l) q(l) \cdot \left(\frac{(i^2 - 2)}{2}\right) \times \frac{1}{((q(l) - p(l) - 2p(l)q(l)) + p(l)\left(\sqrt{2} + i^2 q(l)\right)}, \tag{6}$$

$$p(l) = \frac{l^{1.66}}{7.22 + 2.44 \cdot l^{1.48}}, \tag{7}$$

$$q(l) = \frac{l^{1.92}}{19.14 + 5.25 \cdot l^{1.625}}, \tag{8}$$

$$Ls(i, l) = 4 \times \sqrt{\frac{2(q(l) - p(l)) + p(l)q(l)(i^2 - 4) + \sqrt{2}p(l)}{2(i^2 p(l) - 2q(l)) - 2p(l)q(l)(i^2 - 4) - i^2\sqrt{2}p(l)}}. \tag{9}$$

Analytical expressions make it easy to study the change in the type of the voltage-flux dependence when the system parameters change, as, for example, shown in Fig. 7, *a*. Now let's compare the experimental data with the predictions of the analytical approach (Fig. 7, *b*). It can be seen that in this case, the quality of the obtained approximation can be made quite satisfactory.

The practical significance of the proven analytical approach is determined by the emerging opportunities for

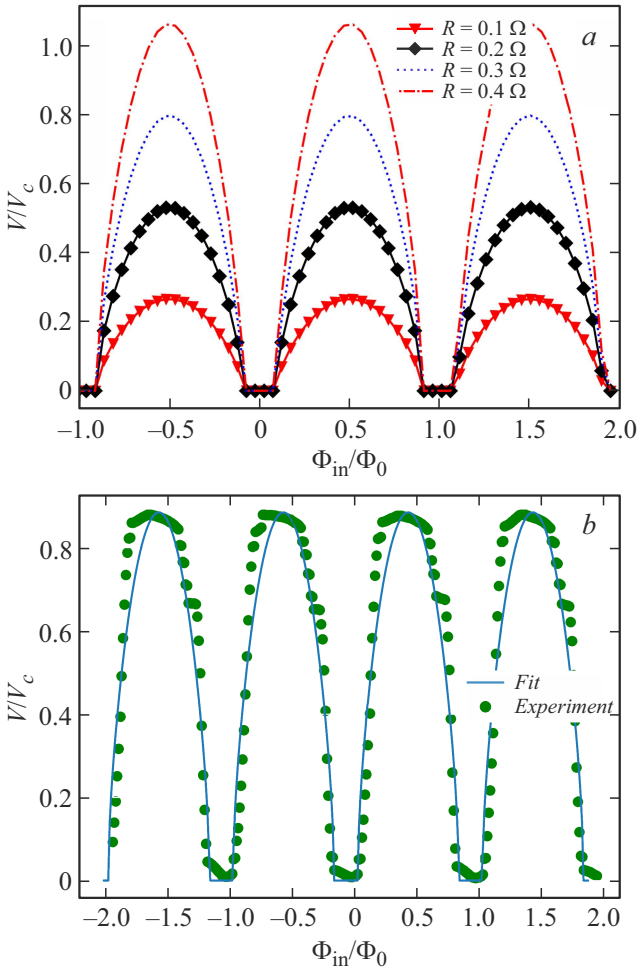

Figure 7. *a* — voltage-flux dependencies at different values of the shunt resistance; parameter values: $L_1 + L_2 = 1.44$ pH, $I_c = 86\,\mu$A; *b* — comparison of the analytical solution (5) for the transport characteristics of the interferometer (curve) and experimental data (points).

designing large arrays of SQUIDs with a high dynamic range necessary for functioning as part of navigation systems. While the shape of the voltage response is one of the most important characteristics of the magnetometers we are interested in, its numerical calculation requires considerable time. In practice, standard specialized software packages for modeling superconducting circuits are not able to cope with circuits containing more than 500 junctions, so complex structures have to be divided into several parts during design. In this regard, the proposed analytical approach to describing the time-averaged characteristics of a SQUID is a valuable solution. The advantage of analytical calculation over numerical calculation becomes obvious if we compare the voltage responses of cells in the SQIF structure.

The voltage on the SQIF structure, without taking into account the finite inductances, will be described by the sum of all voltages (4) on all SQUIDs in the array, and the voltage taking into account the finite inductances is the sum of all voltages (5) also from all SQUIDs. The curve numerically calculated for a SQIF structure containing $N = 20$ SQUIDs is represented by dots in Fig. 8. The SQIF responses for the same structure and for SQIF containing $N = 2000$ SQUIDs, obtained as the sum of the cell responses, are shown in solid lines (the last curve is reduced by 50 times (Fig. 8, blue dotted line). To show the effect of inductors, we calculated the response of the SQIF structure with $N = 20$ by putting $l = 0$ (Fig. 8, solid black curve) and keeping the cell areas unchanged (Fig. 8, red triangles).

We have shown that both the dependences calculated numerically and the results using our analytical approach allow us to obtain an adequate idea of the type of voltage-flux transformation of the SQIF structure. At the same time, the curve calculated in the zero inductance approximation (for $l = 0$) can only provide a rough estimate of the amplitude and shape of the voltage response. When using the analytical approach, we did not obtain a significant difference in the curve calculation time for SQIF structures containing 20 or 2000 SQUIDs. It took about a second on a typical laptop, while the corresponding numerical calculation time would have been at least three orders of magnitude longer. This means that our analytical expressions can be safely used to optimize such complex schemes.

The normalized inductances were taken in the range from 1 to about 7 units: in this range, the analysis [14]

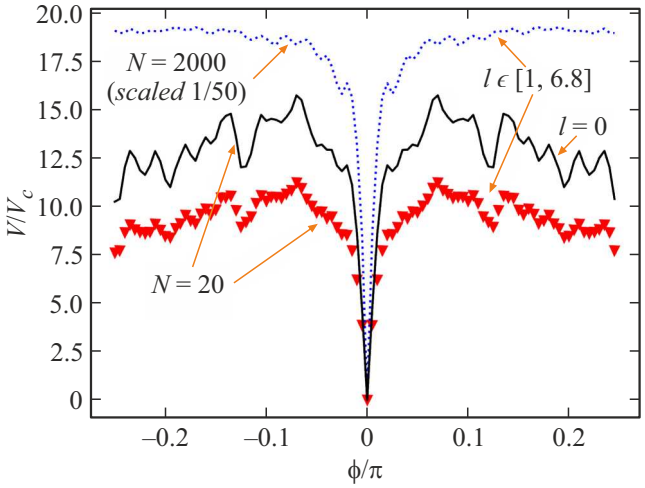

Figure 8. Calculated both numerically (using the brute force method based on the Josephson resistive model of structures) and analytically, the voltage-flux transfer functions for SQIF structures containing series-connected SQUIDs in the amount of 20 (red triangles) and 2000 (blue dotted line) pieces, respectively, the normalized inductances of the SQUIDs are randomly distributed in the range from 1 to 6.8. For comparison, a dependence is given for a SQIF structure of 20 elements with negligible inductances (black solid curve). In the latter case, the calculation using the developed method on a typical personal computer took less than 1 s, which is more than 3 orders of magnitude less than the time required for direct numerical modeling.

allows predicting the shape of the SQUID response. We would like to emphasize that at zero flux, there is a narrow peak in voltage drop to zero for all SQUID circuits with different inductances.

Conclusion

The main characteristics of two-contact SQUIDs and methods for evaluating them based on experimental data were comprehensively studied in this research. The synergy of analytical approaches with practical tests has become the foundation for the precise design of multi-element SQIF structures. Such structures are a complex system in which each individual element may have slightly different parameters of critical current and inductance. Thanks to the analysis of the asymmetry of junctions and parasitic effects at each stage (creation of thin-film structures, installation in a cryostat, current supply and signal removal scheme), it is possible to take into account possible sources of bias instability in navigation systems, reduce parasitic noise and increase the repeatability of results.

It should be noted that the sensitivity $\delta B/\sqrt{\text{Hz}}$ of the entire SQIF array in terms of the magnetic component of the electromagnetic field can be estimated from input noise as follows [15]: $\delta B/\sqrt{\text{Hz}} = 4\sqrt{k_B T R_N}/(dV/dB)$, where k_B is the Boltzmann constant, T is the device operating temperature, R_N is the normal resistance of SQIF structure, dV/dB is the conversion factor. Given that for the considered structure $R_n = 400\,\Omega$, $dV/dB = 6.5 \cdot 10^4\,\text{mV/mT}$, and the operating temperature is 4 K, the sensitivity is $\delta B/\sqrt{\text{Hz}} = 0.89 \cdot 10^{-14}\,\text{T}/\sqrt{\text{Hz}}$. The noise temperature estimates [16] show values slightly higher than background noise for this sensitivity.

Of particular importance is the correct modeling of processes in a superconducting circuit using the Josephson theory (RCSJ model, The Resistively Capacitance Shunted Junction) and modern computing tools. This allows estimating in advance how changes in the geometric dimensions of the contour, the choice of materials, or the connection scheme will affect the resulting voltages, noise spectrum, and operating range of the device. As a result, designers are able to flexibly customize the topology of SQIF structures for specific tasks [17–19] — whether it's high-precision measurements of weak magnetic fields, low-drift navigation, or integration into medical diagnostic devices.

Thus, the methodology demonstrated in the study — from analytics and modeling to experimental tests — opens the way to a new generation of multi-element SQIF systems with even higher sensitivity and stability. Overcoming the problem of bias instability and optimizing the geometry of the base cells will be the key to success in creating promising superconducting sensors for a wide range of applications. In addition, the proven techniques will find their application in works aimed at improving the sensitivity and stability of superconducting magnetometers, improving the operational characteristics of elements of quantum detectors and computing systems [20–24].

Acknowledgments

The equipment of UNU #352529„Cryointegral“ was used for the production of samples.

Funding

This study was financially supported by the Ministry of Science and Higher Education of the Russian Federation (Agreement № 075-15-2024-538).

Conflict of interest

The authors declare that they have no conflict of interest.

References

[1] R. Brady. IEEE Trans. Magn., **17** (1), 861 (1981). DOI: 10.1109/tmag.1981.1061112
[2] I. Khomchenko, P. Navez, H. Ouerdane. Appl. Phys. Lett., **121** (15), (2022). DOI: 10.1063/5.0126680
[3] V.G. Peshekhonov. Gyroscopy and Navigation, **2** (3), 111 (2011). DOI: 10.1134/s2075108711030096
[4] C.W.F. Everitt. In Laser Inertial Rotation Sensors, ed. by S. Ezekiel, G.E. Knausenberger (SPIE, 0157, 1978), p. 175. DOI: 10.1117/12.965483
[5] W.J. Bencze, R.W. Brumley, M.L. Eglington, D.N. Hipkins, T.J. Holmes, B.W. Parkinson, Y. Ohshima, C.W.F. Everitt. Classical Quant. Grav., **32**, 224005 (2015). DOI: 10.1088/0264-9381/32/22/224005
[6] A.V. Rzhevskiy, O.V. Snigirev, Yu.V. Maslennikov, V.Yu. Slobodchikov. Mosc. Univ. Phys. Bull., **75** (4), 336 (2020). DOI: 10.3103/s0027134920040104
[7] R. Stolz, M. Schmelz, V. Zakosarenko, C.P. Foley, K. Tanabe, X. Xie, R. Fagaly. Supercond. Sci. Technol., **34**, 33001 (2021). DOI: 10.1088/1361-6668/abd7ce
[8] S.P. Smith. In Position, Navigation, and Timing Technologies in the 21st Century, ed. by Y.T.J. Morton, F. van Diggelen, J.J.S. Jr., B.W. Parkinson, S. Lo, G. Gao (Wiley, 2020), p. 1413. DOI: 10.1002/9781119458555.ch44
[9] T. Schönau, V. Zakosarenko, M. Schmelz, R. Stolz, S. Anders, S. Linzen, M. Meyer, H.-G. Meyer. Rev. Sci. Instrum., **86** (10), (2015). DOI: 10.1063/1.4933386
[10] V.K. Kornev, I.I. Soloviev, N.V. Klenov, O.A. Mukhanov. IEEE Trans. Appl. Supercond., **21** (3), 394 (2011). DOI: 10.1109/tasc.2010.2095451
[11] R.A. Yusupov, L.V. Filippenko, M.Yu. Fominskiy, V.P. Koshelets. Phys. Solid State, **64** (8), 467 (2022). DOI: 10.1134/s1063783422090086
[12] W.H. Henkels. Appl. Phys. Lett., **32** (12), 829 (1978). DOI: 10.1063/1.89940
[13] M.M. Khapaev, A.Yu. Kidiyarova-Shevchenko, P. Magnelind, M.Yu. Kupriyanov. IEEE Trans. Appil. Supercond., **11** (1), 1090 (2001). DOI: 10.1109/77.919537
[14] I.I. Soloviev, N.V. Klenov, A.E. Schegolev, S.V. Bakurskiy, M.Y. Kupriyanov. Supercond. Sci. Technol., **29** (9), 94005 (2016). DOI: 10.1088/0953-2048/29/9/094005

[15] M.A. GalíLabarias, K.H. Müller, E.E. Mitchell. Phys. Rev. Appl., **17** (6), 064009 (2022). DOI: 10.1088/1361-6668/aa7a52
[16] N.V. Kolotinskiy, V.K. Kornev. Phys. C, **618**, 1354467 (2024). DOI: 10.1103/PhysRevApplied.17.06400910.1016/j.physc.2024.1354467
[17] J. Oppenländer, P. Caputo, Ch. Häussler, T. Träuble, J. Tomes, A. Friesch, N. Schopohl. Appl. Phys. Lett., **83** (5), 969 (2003). DOI: 10.1063/1.1597753
[18] P. Caputo, J. Oppenländer, Ch. Häussler, J. Tomes, A. Friesch, T. Träuble, N. Schopohl. Appl. Phys. Lett., **85** (8), 1389 (2004). DOI: 10.1063/1.1787165
[19] A.V. Shadrin, K.Y. Constantinian, G.A. Ovsyannikov, S.V. Shitov, I.I. Soloviev, V.K. Kornev, J. Mygind. Appl. Phys. Lett., **93** (26), (2008). DOI: 10.1063/1.3058759
[20] M.I. Faley, Y. Liu, R.E. Dunin-Borkowski. Nanomaterials, **11** (2), 466 (2021). DOI: 10.3390/nano11020466
[21] A.G. Shishkin, O.V. Skryabina, V.L. Gurtovoi, S.E. Dizhur, M.I. Faley, A.A. Golubov, V.S. Stolyarov. Supercond. Sci. Technol., **33** (6), 65005 (2020). DOI: 10.1088/1361-6668/ab877c
[22] D.S. Yakovlev, I.A. Nazhestkin, N.G. Ismailov, S.V. Egorov, V.N. Antonov, V.L. Gurtovoi. Symmetry, **15** (2), 550 (2023). DOI: 10.3390/sym15020550
[23] I.A. Nazhestkin, S.V. Bakurskiy, A.A. Neilo, I.E. Tarasova, N.G. Ismailov, V.L. Gurtovoi, S.V. Egorov, S.A. Lisitsyn, V.S. Stolyarov, V.N. Antonov, V.V. Ryazanov, M.Y. Kupriyanov, I.I. Soloviev, N.V. Klenov, D.S. Yakovlev. Adv. Eng. Mater., **27** (5), (2025). DOI: 10.1002/adem.202402385
[24] C. Granata, A. Vettoliere. Phys. Rep., **614**, 1 (2016). DOI: 10.1016/j.physrep.2015.12.001

Translated by A.Akhtyamov